JACS
JOURNAL OF THE AMERICAN CHEMICAL SOCIETY

COMMUNICATION

pubs.acs.org/JACS

Three-Dimensional Pore Evolution of Nanoporous Metal Particles for Energy Storage

Matthew P. Klein,[†] Benjamin W. Jacobs,[‡] Markus D. Ong,[‡] Stephen J. Fares,[‡] David B. Robinson,[‡] Vitalie Stavila,[‡] Gregory J. Wagner,[‡] and Ilke Arslan*[,§]

[†]Department of Mechanical & Aeronautical Engineering, University of California-Davis, Davis, California 95616, United States

[‡]Sandia National Laboratories, Livermore, California 94550, United States

[§]Department of Chemical Engineering and Materials Science, University of California-Davis, Davis, California 95616, United States

Supporting Information

ABSTRACT: A well characterized and predictable aging pattern is necessary for practical energy storage applications of nanoporous particles that facilitate rapid transport of ions or redox species. Here we use STEM tomography with segmentation to show that surface diffusion and grain boundary diffusion are responsible for pore evolution at intermediate and higher temperatures, respectively. This unprecedented three dimensional understanding of pore behavior as a function of temperature suggests routes for optimizing pore stability in future energy storage materials.

The high surface area and unique chemical activity of nanoporous metals are of potential value for catalysis,[1,2] medical treatments,[3] chemical detection,[4] electrical energy storage,[5−9] and hydrogen storage.[10,11] Palladium is a metal that is relevant to all of these areas. In these materials, high surface area can accelerate charging, discharging, or reaction when these are limited by surface processes (due directly to high surface area) or by bulk transport processes, because every point in the material is within a few atoms of an interface.

It is well known that the high surface energy of nanoscale materials (and especially metals) can cause them to restructure at temperatures well below their melting points.[12,13] Coarsening of nanoporous gold has been examined,[14] and pore stability is known to be a strong function of composition.[10,15] It is also expected to be a strong function of size, since material evolution due to diffusion is proportional to variations in local surface curvature,[16,17] and may depend on crystal orientation[18] and the regularity of pore diameter and spacing, which is discussed below. The migration of voids in bulk materials is well studied, especially in stressed environments,[19] but much less so in nanocrystalline or nanostructured materials.

We report the collapse of pores and coarsening at elevated temperatures (∼300−600 °C) on time scales of hours, but long-term aging of materials at more moderate temperatures may also occur, possibly by different mechanisms. It is important, then, to have a thorough understanding of the structural evolution of porous metals as a function of temperature and time, and to understand the mechanism behind the changes.

Here, we aim to address these important challenges by thermally treating nanoporous palladium particles to mimic the aging process, and studying the evolution of the pore structure. Property changes averaged over samples can be obtained through bulk techniques such as physisorption-based surface area measurements and small-angle X-ray or neutron scattering, but these techniques cannot resolve changes on the nanoscale pore level. For higher-resolution analysis, (scanning) transmission electron microscopy ((S)TEM) is usually used to analyze the atomic structure and interfaces of nanoparticles. However, this only provides two-dimensional (2-D) information for an intrinsically three-dimensional (3-D) nanoscale material, and therefore limits the structure−property understanding of these complex materials. Three-dimensional imaging methods have been applied to nanoporous gold by different authors who used various preparation conditions and thermal treatments,[20−22] revealing useful information about pore evolution on pore and grain size scales greater than that considered here.

Here we use electron tomography in the STEM[23] to elucidate the 3-D pore structure as a function of temperature with a resolution of ∼1 nm.[24,25] The palladium particles were synthesized as described previously,[11] and three sets of particles were analyzed. The first set was kept at room temperature as the control sample. The other two sets of particles were respectively heated to 200 and 600 °C, kept at temperature for 30 min, cooled, and then analyzed (we observe that rapid cooling after the heat treatment locks the changed pore structure into place, which then allows for the 3-D imaging to be performed at room temperature).

All experiments were carried out using a JEOL 2010F field emission (S)TEM operating at 200 kV. Samples were heated in situ using a Gatan 652 heating holder. The electron gun valve was closed when possible to minimize electron beam effects on the samples during heating. Tomography was performed using a Fischione 2020 advanced tomography holder. While the tilt range varied for each data set, they all covered ∼130−140° of tilt, with images taken every 1°. The images were aligned by cross correlation and reconstructed by SIRT using the FEI Inspect 3D software. Segmentation and visualization was performed using Avizo Fire. Segmentation was performed semiautomatically (with manual checking of each slice in all three directions for each data set). Note that the reconstructions shown here display information only on the pore structures, i.e. there is no Pd displayed.

Received: January 19, 2011
Published: May 11, 2011

dx.doi.org/10.1021/ja200561w | J. Am. Chem. Soc. 2011, 133, 9144–9147

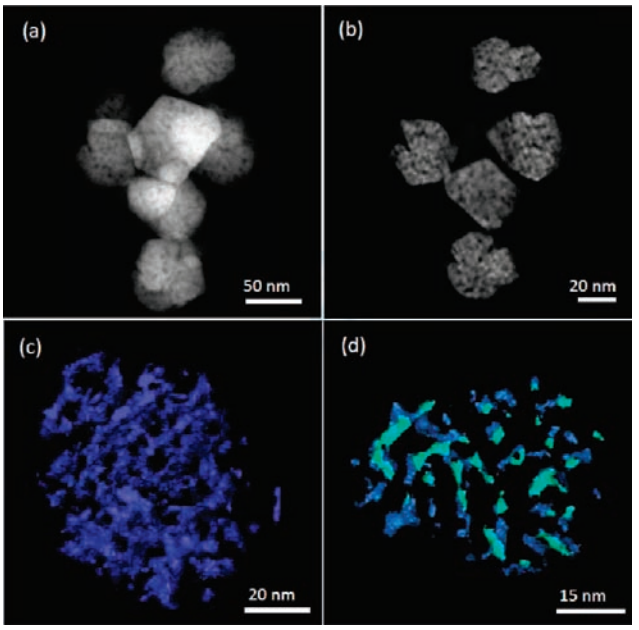

Figure 1. (a) One STEM image from the tilt series of particles with no heat treatment (room temperature control sample); (b) ~1 nm thick slice through the reconstruction; (c) reconstruction of the pore structure of one particle showing that the pores are uniformly ~3 nm (also see Movie 1 in Supporting Information [SI]); (d) ~5 nm slice through the reconstruction in (c) shows the regularity of the pore connections (also see Movie 2 [SI]).

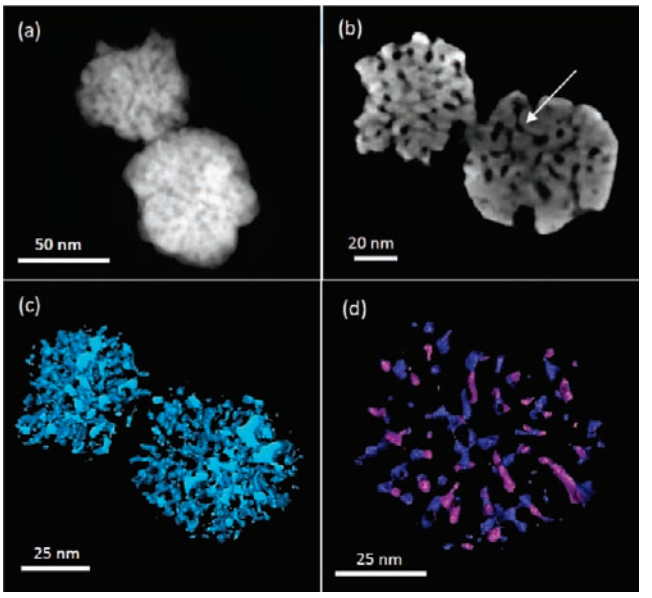

Figure 2. (a) One STEM image from the tilt series of particles heated to 200 °C; (b) ~1 nm thick slice through the reconstruction showing that, while pores still extend to surfaces, they start to swell at pore junctions (see arrow); (c) reconstruction of the pore structure showing the pore connections are larger (also see Movie 3 in SI); (d) ~5 nm slice through the reconstruction in (c) shows the pore connections more clearly (also see Movie 4 [SI]).

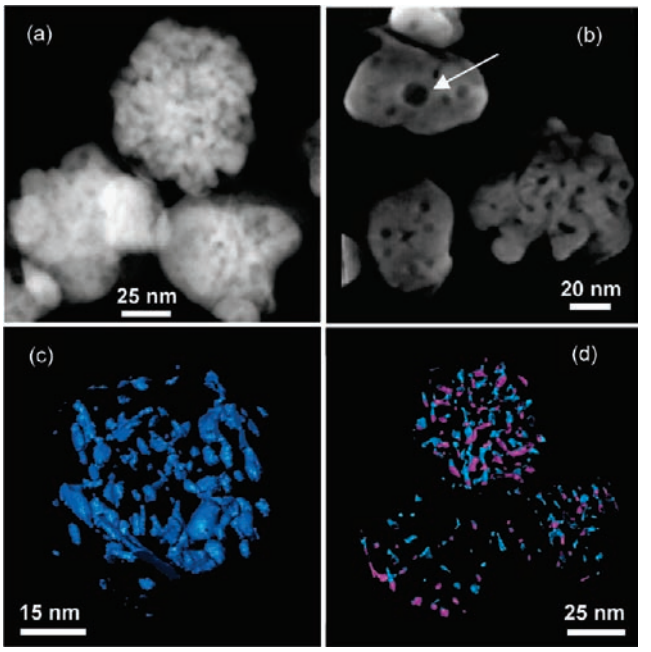

Figure 3. (a) One STEM image from the tilt series of particles heated to 600 °C. (b) ~1 nm thick slice through the reconstruction showing that the pores have now collapsed into bubbles (see arrow). (c) Reconstruction of the pore structure of one particle showing the bubbles more clearly (also see Movie 5 in SI). (d) ~5 nm slice through the reconstruction of all three particles (also see Movie 6).

Figure 1a shows one high-angle annular dark field (HAADF) STEM image from the tilt series of the room temperature sample. The particles are all ~50 nm in diameter. The pores are found to extend through the particles to the surfaces, as seen in the ~1 nm thick slice through the reconstruction in Figure 1b. The bright regions are Pd, and black regions are pores in these two images. Figure 1c (and Movie 1 in SI) shows a 3-D reconstruction of the pore structure of one particle, which has been isolated to display the porosity more clearly. The pores are uniform throughout the particle and ~3 nm in diameter. The pore regularity can be seen more clearly in Figure 1d (and Movie 2 in SI), which displays a ~5 nm thick slice through the reconstruction of Figure 1c. The blue regions in these images are the pores, and the green regions are the exposed surfaces due to the slicing of the reconstruction. Figure 2a shows one HAADF STEM image from the tilt series of the particles heated to 200 °C. Pore evolution from the increased temperature is not readily observed in this image, but is apparent in the reconstructions. Figure 2b shows a ~1 nm slice through the reconstruction. The pores still extend to the surfaces, but the connections between the pores have changed. The most notable effect is that junctions between pores swell into larger, rounder 3−5 nm void spaces, while the rest of the pore becomes thinner. One example of this is indicated by the arrow in Figure 2b. This is seen again more clearly in Figure 2c (and Movie 3 in SI), which shows the reconstruction of the pore structure of the two particles, and in Figure 2d (and Movie 4 in SI), which shows a ~5 nm thick slice cut through one of the reconstructed particle in Figure 2c. The blue regions in these images are the pores, and the purple regions are the exposed surfaces where the reconstruction has been cut. We attribute the pore structure evolution to the relatively high surface energies that exist at junctions. The junctions contain corners that have high curvature and therefore high surface energy. The large gradients in surface energy provide a driving force for surface diffusion toward regions of lower

dx.doi.org/10.1021/ja200561w |*J. Am. Chem. Soc.* 2011, 133, 9144–9147

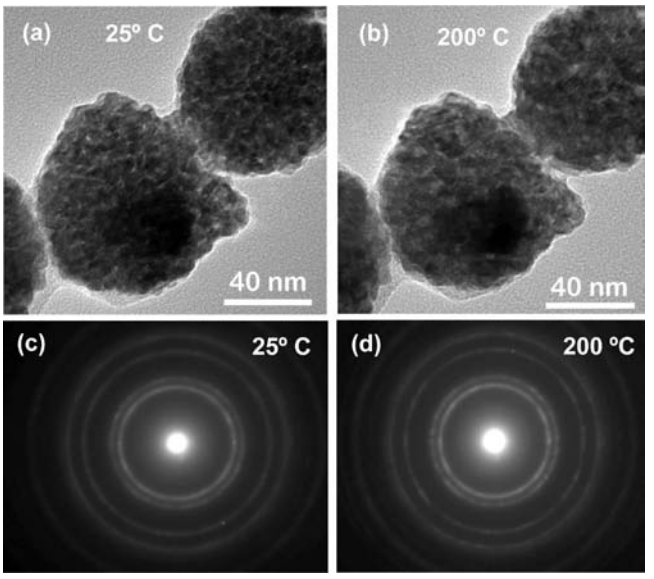

Figure 4. HRTEM images (a,b) and SAED patterns (c,d) comparing particle structure at room temperature and when heat treated to 200 °C.

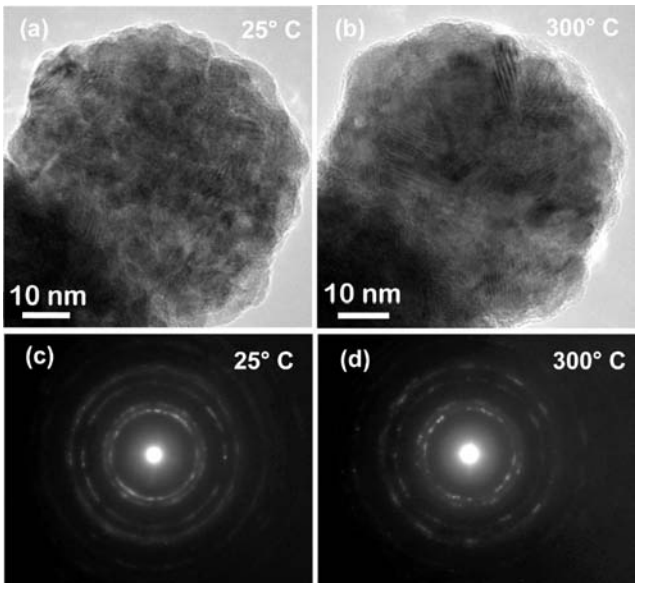

Figure 5. HRTEM images (a,b) and SAED patterns (c,d) comparing particle structure at room temperature and when heat treated to 300 °C.

curvature.[17] The corners become more rounded, and material is redistributed along the surface, causing further variation in pore diameter.

Figure 3a shows one HAADF STEM image from the tilt series of the particles heated to 600 °C. Even after heating to this higher temperature, pore structure evolution is still not apparent in the STEM images. However, the ∼1 nm thick slice of the reconstruction in Figure 3b clearly shows that some of the pores have now become 5−10 nm internal bubbles (one example is highlighted by the arrow). This can also be seen in the 3-D reconstruction of one particle in Figure 3c (and Movie 5 in SI), and in the ∼5 nm thick slice through the reconstruction in Figure 3d (and Movie 6 in SI). Most of the pore space is gone, and the overall pore volume is reduced. This volume reduction suggests that the mechanism for pore evolution is different from that at lower temperatures. When a long cylindrical pore connected to the surface collapses under surface diffusion, it is expected to first pinch off near the surface, similar to the behavior of metallic nanowires that has been described theoretically[17] and experimentally.[26] The resulting internal voids would evolve with a constant volume, which is not observed. This suggests that a bulk diffusion mechanism, such as that along grain boundaries, is active at higher temperatures in addition to surface diffusion.

We observe some variation of the pore evolution between the three adjacent particles heated to 600 °C. We believe that this is due to sensitivity of the collapse mechanism to geometric details. Rearrangement of one unstable feature can destabilize a neighboring region, so the pore collapse mechanism can be expected to be self-reinforcing, causing most of a particle's pores to collapse nearly all at once, and at different times from other particles.

To compare the different pore evolution mechanisms observed in the tomography data, bright-field TEM and selected area electron diffraction (SAED) patterns were used to analyze particles at room temperature and particles heated to 200 and 300 °C. Images a and b of Figure 4 show before and after images of particles heated to 200 °C. Their corresponding SAED patterns in images c and d of Figure 4, which sample a larger number of particles, show some relative change indicated by the slight increase in spots (decrease in the ring pattern) for the particles heated to 200 °C. Powder X-ray diffraction on a 20-mg scale sample (see SI) indicates an average grain size of 17 nm at room temperature and 20 nm after heating at 200 °C, by Rietveld analysis. From these observations, we believe that there is no significant bulk diffusion mechanism that influences pore structure at these temperatures.

Figure 5 shows TEM images and SAED patterns of particles before and after heating to 300 °C. The size of crystal grains is observed to increase after heating to 300 °C, as evidenced by the images and the relative increase in spots (and decrease of rings) in the SAED patterns in c and d of Figure 5 (which sample a larger number of particles). A grain size of 32 nm is derived from X-ray diffraction upon heating to 600 °C (see SI).

These two data sets (Figures 4 and 5) illustrate that above 200 °C, grain growth becomes evident; therefore, transport of atoms along grain boundaries can occur. These regions are expected to have barriers to diffusion that are greater than that of surface atoms, but lower than that of bulk atoms.[27] Transport at grain boundaries can allow growth of one grain at the expense of another, or at the expense of a pore. Transport of atoms from pore surfaces to grain boundaries, or the reverse, would cause pores to change size, their overall orientation, or both.

STEM tomography is a unique tool capable of providing reliable information on porosities in nanomaterials on the 1-nm scale or larger. By studying Pd particles heat treated to different temperatures in 3-D, we are able to ascertain that pore junctions are where the collapse mechanism begins. We observe that surface diffusion occurs first at lower temperature, where the pore junctions start to swell. As the temperature continues to increase, grains in the particles begin to coalesce, while surface diffusion may continue. The combined processes provide a route for the pores to meet and collapse into larger bubbles. In this stage, grain boundary diffusion causes more drastic effects, which can reorient entire pores. The collapse can be sensitive to parameters such as pore size, grain size, grain orientation, and their interrelationship. These observations suggest a route to improve pore stability and higher temperature applications for

future energy storage materials by changing the initial structure to have more regular pores with the fewest junctions possible to prevent premature pore collapse.

■ ASSOCIATED CONTENT

Supporting Information. Powder X-ray diffraction data are in Part 1. Movies 1−6 are 3-D animations of the tomograms using the figures in this paper as a starting point. Movie 1 is a reconstruction of the pore structure of only one particle from the tilt series at room temperature, showing that the pores are uniform and ∼3 nm in diameter. Movie 2 is a ∼5 nm slice through the reconstruction in Movie 1, showing the uniformity of the interconnections of pores at room temperature more clearly. The blue regions are the pores, and the green regions are the surfaces where the tomogram has been cut. Movie 3 is a reconstruction of the pore structure of both particles from the tilt series at 200 °C , showing that the pores swell at the junctions, with the rest of the pore thinning out. Movie 4 is a ∼5 nm slice through the reconstruction in Movie 3, showing the swelling of the pore junctions more clearly. The blue regions are the pores, and the purple regions are the surfaces where the tomogram has been cut. Movie 5 is a reconstruction of the pore structure of only one particle from the tilt series at 600 °C, showing that the pores have finally separated, leaving bubbles behind in the Pd (Pd not shown). Movie 6 is a ∼5 nm slice through all three particles at 600°C, showing the bubble formation more clearly in two of the three particles. The blue regions are the pores, and the purple regions are the surfaces where the tomogram has been cut. This material is available free of charge via the Internet at http://pubs.acs.org.

■ AUTHOR INFORMATION

Corresponding Author
iarslan@ucdavis.edu

■ ACKNOWLEDGMENT

This work was supported in part by Sandia's Truman Fellowship and other funds from the Laboratory Directed Research and Development program. Sandia National Laboratories is a multiprogram laboratory operated by Sandia Corporation, a wholly owned subsidiary of Lockheed Martin Corporation, for the U.S. Department of Energy's National Nuclear Security Administration under contract DE-AC04-94AL85000.

■ REFERENCES

(1) Wittstock, A.; Zielasek, V.; Biener, J.; Friend, C. M.; Baumer, M. *Science* **2010**, *327* (5963), 319–322.
(2) Denuault, G.; Milhano, C.; Pletcher, D. *Phys. Chem. Chem. Phys.* **2005**, *7* (20), 3545–3551.
(3) Gittard, S. D.; Pierson, B. E.; Ha, C. M.; Wu, C. A. M.; Narayan, R. J.; Robinson, D. B. *Biotechnol. J.* **2010**, *5* (2), 192–200.
(4) Lang, X. Y.; Chen, L. Y.; Guan, P. F.; Fujita, T.; Chen, M. W. *Appl. Phys. Lett.* **2009**, *94*, 21.
(5) Bartlett, P. N.; Gollas, B.; Guerin, S.; Marwan, J. *Phys. Chem. Chem. Phys.* **2002**, *4* (15), 3835–3842.
(6) Elliott, J. M.; Owen, J. R. *Phys. Chem. Chem. Phys.* **2000**, *2* (24), 5653–5659.
(7) Robinson, D. B.; Wu, C. A. M.; Jacobs, B. W. *J. Electrochem. Soc.* **2010**, *157* (8), A912–A918.
(8) Robinson, D. B.; Wu, C. A. M.; Ong, M. D.; Jacobs, B. W.; Pierson, B. E. *Langmuir* **2010**, *26* (9), 6797–6803.
(9) Yamauchi, Y.; Momma, T.; Yokoshima, T.; Kuroda, K.; Osaka, T. *J. Mater. Chem.* **2005**, *15* (20), 1987–1994.
(10) Robinson, D. B.; Langham, M. E.; Fares, S. J.; Ong, M. D.; Jacobs, B. W.; Clift, W. M.; Murton, J. K.; Hjelm, R. P.; Kent, M. S. *Int. J. Hydrogen Energy* **2010**, *35* (11), 5423–5433.
(11) Robinson, D. B.; Fares, S. J.; Ong, M. D.; Arslan, I.; Langham, M. E.; Tran, K. L.; Clift, W. M. *Int. J. Hydrogen Energy* **2009**, *34* (13), 5585–5591.
(12) Lewis, L. J.; Jensen, P.; Barrat, J. L. *Phys. Rev. B* **1997**, *56* (4), 2248–2257.
(13) Campbell, C. T.; Parker, S. C.; Starr, D. E. *Science* **2002**, *298* (5594), 811–814.
(14) Ji, C. X.; Searson, P. C. *J. Phys. Chem. B* **2003**, *107* (19), 4494–4499.
(15) Snyder, J.; Asanithi, P.; Dalton, A. B.; Erlebacher, J. *Adv. Mater.* **2008**, *20* (24), 4883–4886.
(16) Nichols, F. A.; Mullins, W. W. *J. Appl. Phys.* **1965**, *36* (6), 1826.
(17) Nichols, F. A. *J. Mater. Sci.* **1976**, *11* (6), 1077–1082.
(18) Santala, M. K.; Glaeser, A. M. *Acta Mater.* **2008**, *56* (9), 1967–1980.
(19) Nichols, F. A. *J. Nucl. Mater.* **1969**, *30* (1−2), 143–165.
(20) Chen, Y. C. K.; Chu, Y. S.; Yi, J.; McNulty, I.; Shen, Q.; Voorhees, P. W.; Dunand, D. C. *Appl. Phys. Lett.* **2010**, *96*, 043122.
(21) Fujita, T.; Qian, L. H.; Inoke, K.; Erlebacher, J.; Chen, M. W. *Appl. Phys. Lett.* **2008**, *92*, 251902.
(22) Rosner, H.; Parida, S.; Kramer, D.; Volkert, C. A.; Weissmuller, J. *Adv. Eng. Mater.* **2007**, *9* (7), 535–541.
(23) Midgley, P. A.; Weyland, M. *Ultramicroscopy* **2003**, *96* (3−4), 413–431.
(24) Arslan, I.; Yates, T. J. V.; Browning, N. D.; Midgley, P. A. *Science* **2005**, *309* (5744), 2195–2198.
(25) Arslan, I.; Walmsley, J. C.; Rytter, E.; Bergene, E.; Midgley, P. A. *J. Am. Chem. Soc.* **2008**, *130* (17), 5716–5719.
(26) Karim, S.; Toimil-Molares, M. E.; Balogh, A. G.; Ensinger, W.; Cornelius, T. W.; Khan, E. U.; Neumann, R. *Nanotechnology* **2006**, *17* (24), 5954–5959.
(27) Shewmon, P. G. In *Transformations in Metals* J. Williams Book Co.: Jenks, OK, 1983.